# Simplifying the First Order Reversal Curves method for molecular magnets by using a calorimetric approach

Diana Plesca, Cristian Enachescu, Radu Tanasa, Alexandru Stancu, Denis Morineau, Marie-Laure Boillot

# Simplifying the First Order Reversal Curves method for molecular magnets by using a calorimetric approach

Diana Plesca[a], Cristian Enachescu[a], Radu Tanasa[a,*], Alexandru Stancu[a], Denis Morineau[b], Marie-Laure Boillot[c]

[a] *Faculty of Physics, "Alexandru Ioan Cuza" University, 700506, Iasi, Romania*

[b] *Institut de Physique de Rennes, CNRS, Université de Rennes, UMR 6251, 35042 Rennes, France*

[c] *Institut de Chimie Moléculaire et des Matériaux d'Orsay, CNRS, Université Paris-Saclay, UMR 8182, 91400 Orsay, France*

*Corresponding author: radu.tanasa@uaic.ro

**ABSTRACT**

Here we present an alternative to the classical SQUID magnetometric measurements for The First-Order Reversal Curve (FORC) diagram approach by using Differential Scanning Calorimetry (DSC) experiments. After presenting the main results, advantages and drawbacks of the magnetometric FORCs, we introduce the calorimetric method and we argue that, while the results are similar to magnetometric method, it leads to a simplification of the needed mathematical computations. The method is exemplified by both experimental data and mean-field simulations.

## INTRODUCTION

The First-Order Reversal Curves (FORCs) belong to a distinct category of minor hysteresis loops, for which the sweep of the input parameter is reversed once from one of the branches of the major hysteresis loop. The FORC method has emerged as a valuable tool for studying the hysteresis behaviour in various materials. Initially used for analysing ferromagnetic materials,[1] it has expanded to encompass a diversity of hysteretic phenomena observed in ferroelectricity[2], geology[3] and many others. Over the past decade, the FORC method has provided valuable insights into understanding the properties of spin-crossover compounds[4-10] as well.

Early investigations based on the FORC method in spin-crossover (SC) complexes primarily focused on examining thermal hysteresis. These studies effectively characterized the properties of spin-like domains using physical parameters like the coercivity and the bias from the thermal hysteresis loops which respectively correspond to intra- and inter-domain interactions[11] or to distributions of energy gaps[12]. In recent years, intensive studies have been performed on the effects of the environment (in the form of other SC particles, polymer matrices or substrates) on the changes of hysteretic properties of SC systems. Consequently, requirement for more advanced experimental techniques that can efficiently probe the environment influence on the SC switching behaviour is in high demand. In addition to other techniques, FORC method emerges as one of the most suitable options due to its capability as a highly sensitive detector of interaction changes.[13, 14]

The main problem in the numerical calculation of the FORC diagrams implies the computation of the second-order derivative of the output parameter, which in SC field is the high spin (HS) fraction, $n_{HS}$ – the fraction of molecules in the HS state. The second-order derivative of a function with discrete noise-contaminated data increases

the noise that is inevitably present in the measurements. Although the noise may not particularly be evident in the original data, it is more noticeable in the derivative.[15]

To overcome the limitations of the conventional approach for obtaining FORC distributions, we propose a more direct method when calorimetric measurements are available. By leveraging the fact that heat capacity is already related to the first derivative of high spin fraction with respect to temperature, only a single derivative is required to derive the FORC distributions. The idea of using a single derivative to obtain the FORC diagram was theoretically mentioned over a decade ago in a study on voltammetric current in the electrochemical FORC method.[16] However, excepting a short collateral discussion in one previous paper on the behaviour of spin crossover molecules embedded in matrices[11], practical implementation of this concept has not been explored until now.

## 1. EXPERIMENTAL RESULTS

### A. Magnetometric measurements

The vast majority of FORC measurements for spin crossover compounds have been made on SQUID magnetometry. A typical compound used in these studies is the coordination polymer $[Fe(btr)_2(NCS)_2]\cdot H_2O$ (btr=4,4'-bis(1,2,4-triazole)], which has a 2D network structure.[17] The iron atom is related in a plane to four btr ligands and well below room temperature SC displays a large thermal hysteresis loop – sign of a first order phase transition.

In the SQUID magnetometric measurements for SC compounds, the heating/cooling types of FORC experiments should be distinguished, according to the sign of the thermal variations. The measurements start at a sufficiently high/low temperature such that the high/low temperature (HS/LS) domain structure is saturated. Then, the temperature is lowered/ raised until a given temperature $\left(T_R/T_R^*\right)$, named the

reversal temperature, and afterward raised/lowered till reaching full HS/LS structures, in the heating/cooling mode, respectively. The experiment is repeated for several values of $(T_R/T_R^*)$ and $n_{HS}(T_R,T)/n_{HS}(T_R^*,T)$ values form the FORC data (T is the temperature at which the $n_{HS}$ is measured while $T_R$ and $T_R^*$ are the reversal temperatures on the cooling / heating branch of the thermal hysteresis loop). Usually, at the end, the data points will be plotted on an evenly spaced grid in the $(T, T_R)$ coordinate system.

Mathematically, a FORC distribution is defined as the second order mixed derivative of the output parameter:

$$\rho(T_R,T) = -\frac{\partial^2 n_{HS}(T_R,T)}{\partial T_R \partial T} \quad \text{and} \quad \rho(T_R^*,T) = +\frac{\partial^2 n_{HS}(T_R^*,T)}{\partial T_R^* \partial T} \qquad (1)$$

for heating (i.e. FORC heating) and cooling (i.e. FORC cooling) modes, respectively.

The contour plot of the FORC distribution is named a FORC diagram.

The FORCs and FORC diagrams measured experimentally for the coordination polymer $[Fe(btr)_2(NCS)_2]\cdot H_2O]$ are presented in Fig. 1, both for heating and cooling modes. To analyse the FORC distributions, we represent them in the two half planes, separated by the $T_R = T_R^* = T$ line, with the heating diagram below and the cooling diagram above this line.

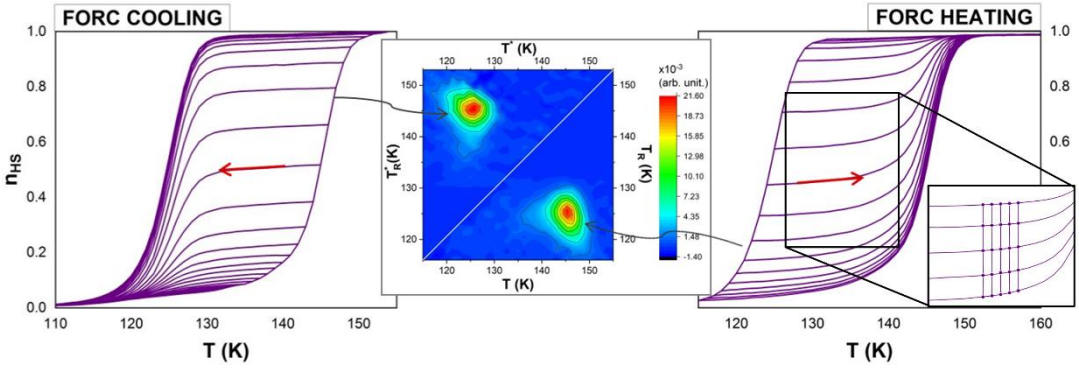


**Fig. 1:** FORC curves and diagrams for $Fe(btr)_2(NCS)_2\cdot H_2O$ in the cooling and heating mode for magnetometric measurements (temperature sweeping rate 0.3 K $min^{-1}$).

Inset right panel: a subset of five consecutive heating FORCs where the circled points represent a $5 \times 5$ array of data in $(T, T_R)$ plane.

It is important to recall that, the evaluation of the FORC distribution at a point P on the $(T, T_R)$ grid, it is based on a local square lattice of data points with P at the center. The number of the points on the local lattice is $(2\,SF + 1)^2$, where SF is the smoothing factor that can be set at 2 for well-behaved samples or higher for samples with low signal to noise ratios.[18] For $SF = 2$ smoothing is performed across a $5 \times 5$ array of data (see Fig. 1, inset). Next, the $n_{HS}$ fraction at these data points is fitted with a polynomial surface in a least-squares manner (standard FORC method) and the coefficient of the mixed term is the FORC distribution at point P.[18] One drawback of this approach is the loss of many details for a set of noisy data where a high value for smoothing factor must be used. Also, the diagram will not show the first and last SF curves which could result in a trimmed picture.

The FORC diagram in the switching temperature plane $(T,\ T_R)$ does not provide directly the physical information needed for the characterization of the spin transition material. An alternative solution is to convert the FORC diagram from the temperature plane to a physical parameters plane: (bias, coercivity) coordinates, as illustrated in Fig. 2, which roughly correspond to the energy gap $\Delta$ and intra-domain interaction J.[19]

The transformation relations for bias b and coercivity c are:

$$b = \frac{T + T_R}{2} \quad \text{and} \quad c = \frac{T - T_R}{2} \tag{2}$$

The bias (the equilibrium temperature $T_{1/2}$ value) reflects the effect of internal stresses which affects the energy gap value ($\Delta$). These internal stresses may be due to

elastic interactions between spin-like domains and therefore the bias distribution can be considered as being caused by some kind of inter-domain interactions.

The coercivity (the width of the thermal hysteresis loop) shows the strength of intra-domain interactions.[20]

By definition, $T \geq T_R$, so $\rho(T_R,T)$ is only well defined for $c \geq 0$, so that a FORC diagram is confined to the right-hand half plane. FORC diagrams are often rotated counterclockwise by 45° from the $(T_R,T)$ coordinate view, so that the x-y cartesian axes are the c and b axes of the FORC diagram.

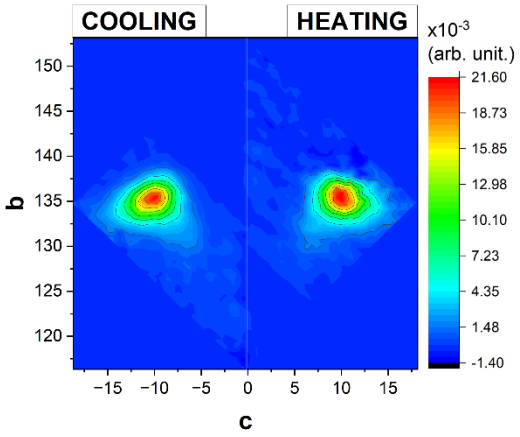


**Fig. 2:** FORC diagram in (bias, coercivity) coordinate plane for $Fe(btr)_2(NCS)_2 \cdot H_2O$ in the cooling and heating mode for magnetometric measurements.

## B. **Calorimetric measurements**

Calorimetric measurements are used as a complementary method to quantitatively evaluate the spin-crossover features. The Differential Scanning Calorimetry (DSC) measures the heat flow associated with the speed of progress of the spin transition, rather than the instantaneous fraction of transformed spins measured by magnetometric methods (see also supplementary material). It is sensitive to the phase transformations

of SC but moreover it detects crystallization, melting and glass transitions of the embedding matrix in case of composite structures.[11]

The recording of calorimetric FORCs as heat capacity profiles (Fig. 3) opened the possibility to represent FORC distributions for calorimetric data. However, there is an important difference compared to the standard method for obtaining FORC distribution; as the heat flow (denoted with H(T)) already corresponds to the first derivative of $n_{HS}$ with the temperature, only a single derivative is necessary to obtain the FORC distributions:

$$\rho(T, T_R) = -\frac{\partial H(T)}{\partial T_R} \quad \text{and} \quad \rho\left(T, T_R^*\right) = +\frac{\partial H(T)}{\partial T_R^*} \tag{3}$$

for heating and cooling modes.

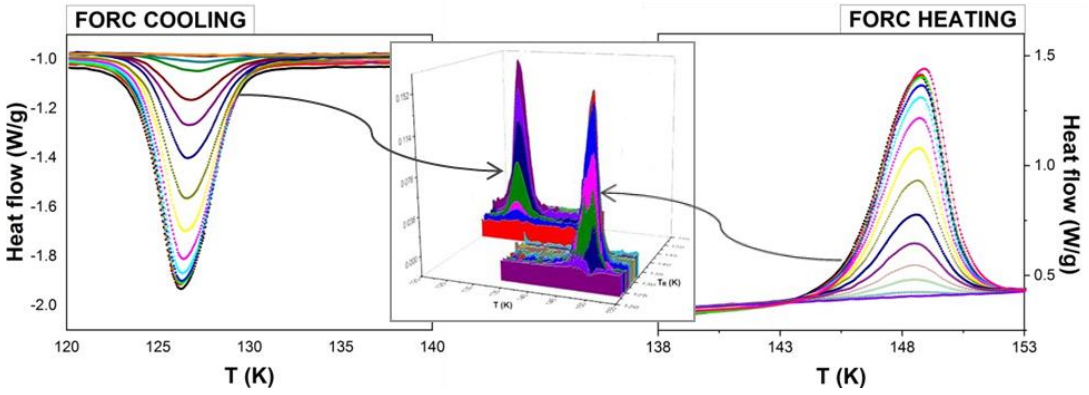


**Fig. 3:** FORC thermograms (sides) and FORC distributions (in the middle) for $Fe(btr)_2(NCS)_2 \cdot H_2O$ polycrystallites in the cooling and heating mode for calorimetric measurements (endothermic signal up).

By integrating the thermogram with respect to the temperature, we obtain the FORC curves (Fig. 4) similar to the ones from magnetometric measurements (see also Fig. 1).

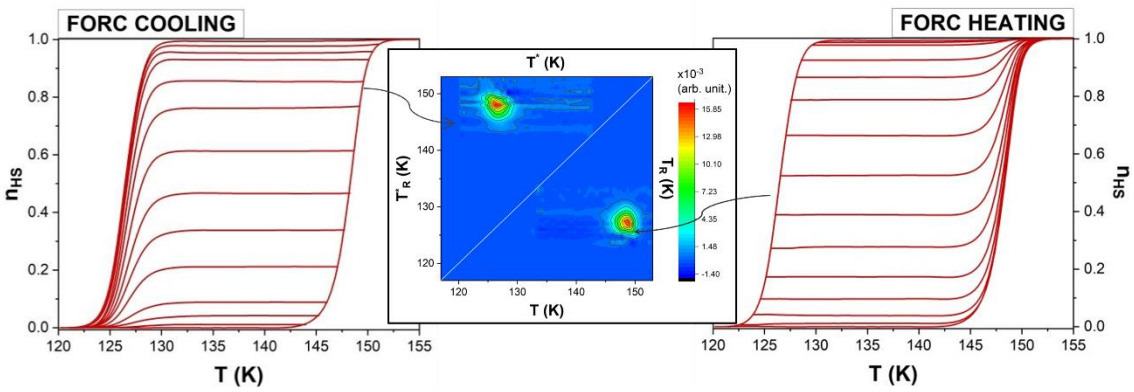


**Fig. 4:** FORC curves and diagrams for $Fe(btr)_2(NCS)_2 \cdot H_2O$ in both heating and cooling modes for calorimetric measurements.

There is a subtle difference of the calorimetric measurement compared to the magnetometric one. The specificity of this experiment is the quite large temperature step between two consecutive reversal temperatures (typically between 0.5 and 1 K compared to 0.1 – 0.2 K for the magnetometric one), due to the necessity to record all curves during a single continuous experimental run to ensure being in the same conditions. Hence the number of consecutive FORC curves measured in a single experiment (ca. 15-20 when applying a temperature ramp of 1 K/min) is determined by the limited autonomy duration in liquid nitrogen of the cooling system. In the same time the temperature step for a given value of the reversal temperature should be small to obtain smooth curves (representing the first derivative of the HS fraction, as we have explained before). Therefore, the grid for FORC evaluation based on polynomial fitting is not anymore evenly spaced which could generate artificially structure in the diagram but also incomplete diagrams due to the loss of first and last $SF$ curves as we discuss it in the previous section, would be generated. These drawbacks are easily avoided in the calorimetric measurements where only one single derivative is needed for the diagram to be obtained.

## 2. SIMULATIONS

To understand and explore more in depth the calorimetric FORCs, simulation approach in the framework of an Ising-like model was used.

The Ising model for spin crossover complexes associates a fictitious spin ($\sigma_i = \pm 1$ i.e. HS $\rightarrow$ +1 and LS $\rightarrow$ -1 state) to each molecule situated in a rectangular configuration, (see Fig. 5) and introduces short and long range intermolecular interactions through the following Ising-like Hamiltonian:

$$H = \frac{1}{2}\sum_i(\Delta - k_B T \ln g)\sigma_i - J\sum_{i,j}\sigma_i\sigma_j - G\sum_i \sigma_i<\sigma> \quad (4)$$

with $\Delta$ being the energy difference, $k_B$ Boltzmann constant, T the system temperature, $\sigma_i$ the fictitious spin, $g = \frac{g_{HS}}{g_{LS}}$ the degeneracy ratio between the two states related to the entropy $\Delta S = \ln g$, J the short-range interaction and G the long-range interaction constants. The fraction $n_{HS}$ is expressed as a function of the "fictitious magnetization"

$$n_{HS} = \frac{1 + <\sigma>}{2} \quad (5)$$

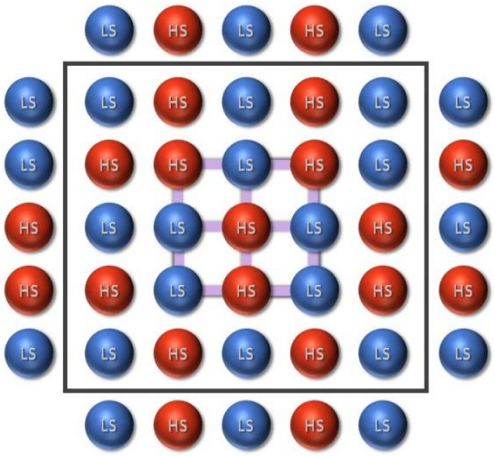


**Fig. 5:** Schematic representation of an Ising-like system with periodic boundary conditions, containing HS (spin up – red molecules) and LS molecules (spin down – blue molecules).

The evolution of the system follows Monte Carlo Arrhenius dynamics[21], in which the transition probabilities are modulated by an activation energy $E_A$.

$$\begin{cases} P_{HS \to LS} = \frac{1}{\tau} e^{\frac{\Delta - k_B T \Delta S}{2 k_B T}} e^{-\frac{E_A + 2G\langle\sigma\rangle + 2J \sum \sigma_{neighbors}}{k_B T}} \\ P_{LS \to HS} = \frac{1}{\tau} e^{-\frac{\Delta - k_B T \Delta S}{2 k_B T}} e^{-\frac{E_A - 2G\langle\sigma\rangle - 2J \sum \sigma_{neighbors}}{k_B T}} \end{cases} \quad (6)$$

where $\tau$ is a scaling constant and $\Delta S$ entropy variation. The term $\sum \sigma_{neighbors}$ is the sum of the fictitious spin values of the first order neighbors of the molecules whose transition probability is calculated.

The Monte Carlo algorithm is the following[22]:

(i) We consider all the molecules in the HS (for heating branch) or LS state (for cooling branch);

(ii) For a random chosen molecule in the system, we calculate the transition probability;

(iii) If this probability is larger than a random generated number r $\epsilon$ (0, 1), then the transition occurs and the particle switches to the new spin state; if it is smaller than r, the particle preserves its spin state

(iv) We repeat the steps (ii) and (iii) for a number of molecules equal to all the particles in the system. This concludes a Monte Carlo step (MCS).

Multiple Monte Carlo steps are performed to establish the equilibrium state of the system. The more steps we consider, the closer the simulation will describe the real equilibrium state. Moreover, we showed in the past that more realistic simulation results are obtained when the parameters are distributed.[12]

By using this method, we can calculate the value of the high spin fraction for a certain temperature range (Fig. 6), but more interestingly we can directly obtain the calorimetric curves (Fig. 7), where the heat flow ($\Delta H$) is proportional to the number of molecules that switch their spin state at each temperature ($\Delta n = n_{HS \to LS} - n_{LS \to HS}$).

$$\Delta H = \Delta H_{LS \to HS} - \Delta H_{HS \to LS} \sim \Delta n \quad (7)$$

The parameters considered for the simulation for a quadratic system (100 x 100 particles), with periodic boundary conditions, were: $\Delta S = 7$, $E_A = 400$ K, $k_B = 1$, G = 0 and the Gaussian distributions for $\Delta$, centered ($\mu_\Delta$) to 1000, with a standard deviation ($\sigma_\Delta$) of 200 and constant values for J = 50 K (Fig. 6a and Fig. 7a) or 55 K (Fig. 6b and Fig. 7b).

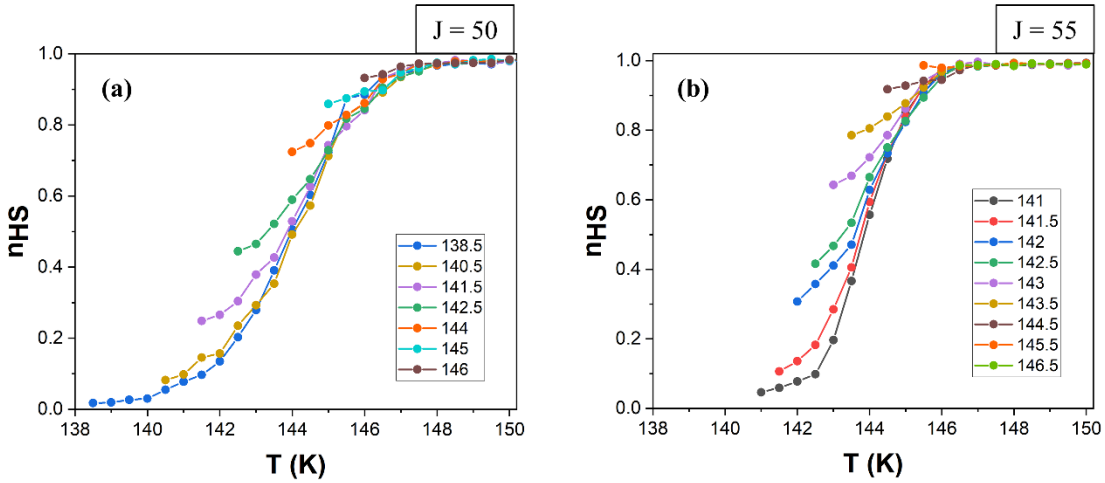


**Fig. 6:** Simulated magnetometric FORCs in the heating mode for $\Delta S = 7$, $E_A = 400$ K, $k_B = 1$, $G = 0$, $\mu_\Delta = 1000$, with $\sigma_\Delta = 200$ and a) J = 50 and b) J = 55. Lines are guides for the eyes.

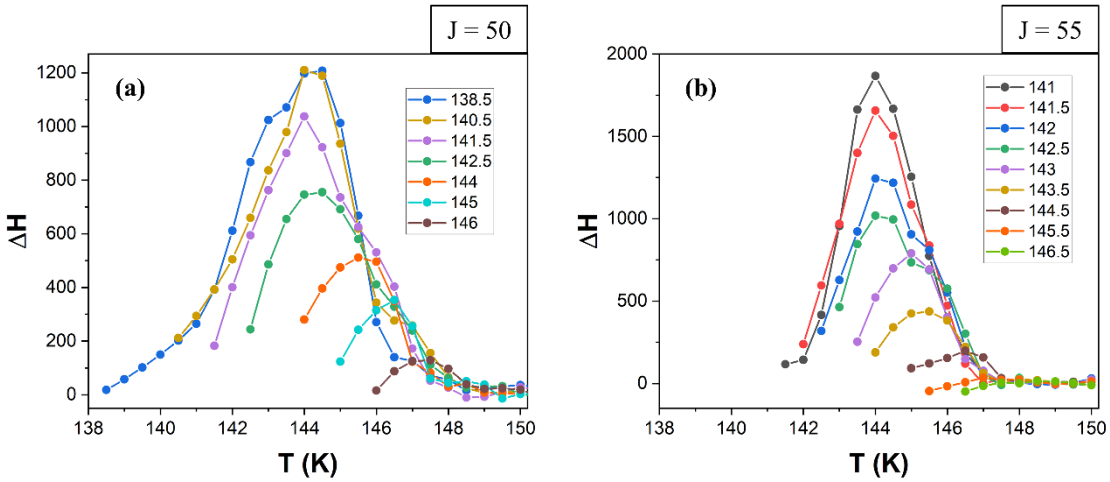


**Fig. 7:** Simulated calorimetric data (thermograms) in the heating mode for $\Delta S = 7$, $E_A = 400$ K, $k_B = 1$, $G = 0$, $\mu_\Delta = 1000$, with $\sigma_\Delta = 200$ and a) J = 50 and b) J = 55. Lines are guides for the eyes.

To further analyse the calorimetric method in comparison to the classical magnetometric one, we represented a magnetic hysteresis loop and its corresponding calorimetric simulation. As we can see in Fig. 8, the calorimetric peak is where there is a rapid increase in the high spin fraction, at $T_{1/2}$ (equilibrium/transition temperature –

temperature at which the number of molecules in the high spin state is equal to the number of molecules in the low spin state – $n_{HS}$ = 0.5).

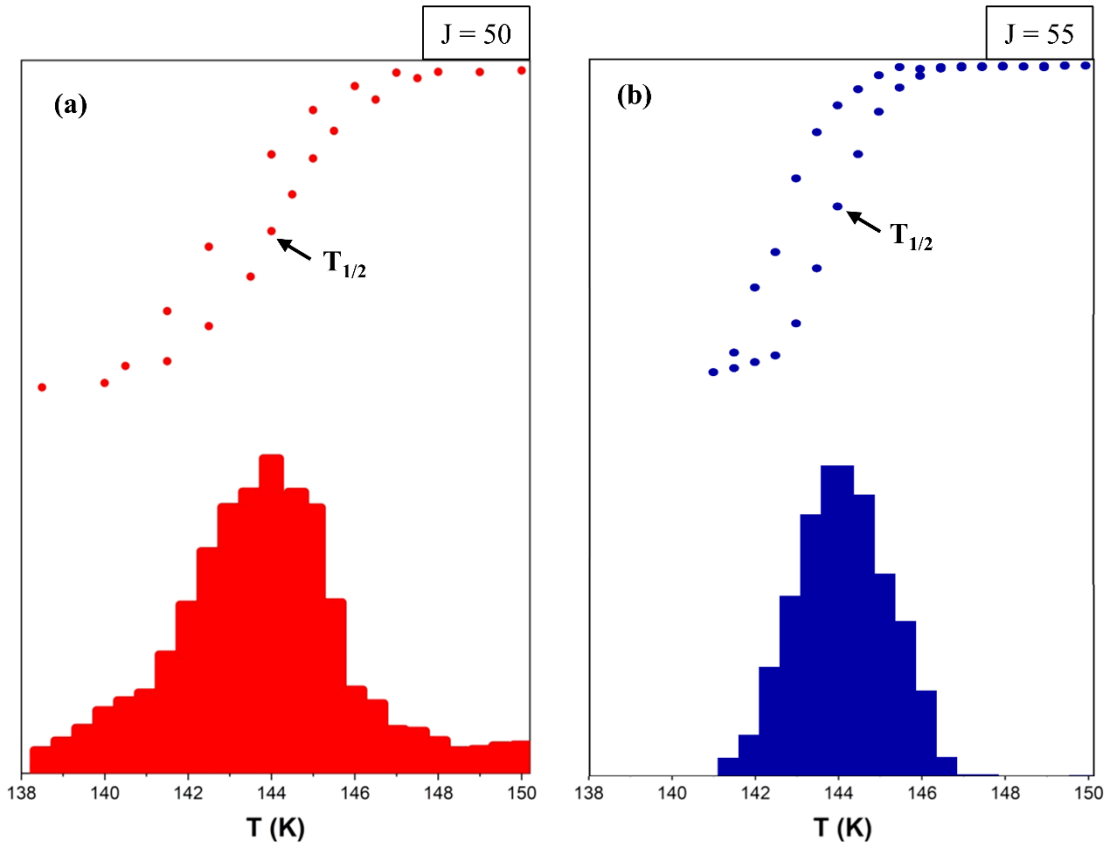


**Fig. 8:** Comparison between a major hysteresis loop (magnetometric data – up) and a heat capacity profile, simulated in heating mode (calorimetric data – down) for ΔS = 7, $E_A$ = 400 K, $k_B$ = 1, G = 0, $\mu_\Delta$ = 1000, with $\sigma_\Delta$ = 200 and a) J = 50 and b) J = 55.

The ($n_{HS}$, T) data was plotted as FORC diagrams using the polynomial fitting (i.e. standard FORC method) for smoothing factor $SF = 3$, i.e. 49 nearest neighbors for each input point (Fig. 9a and Fig. 10a).

FORC diagrams were also obtained from calorimetric data by calculating the derivative of the smoothed values of the heatflow (Fig. 9b and Fig. 10b). The similarities between these FORC diagrams are a solid argument for the approach proposed here to evaluate FORC thermograms. While in a simulation, we could choose

between both methods, for the experimental data only the direct calculation of the derivative should be employed.

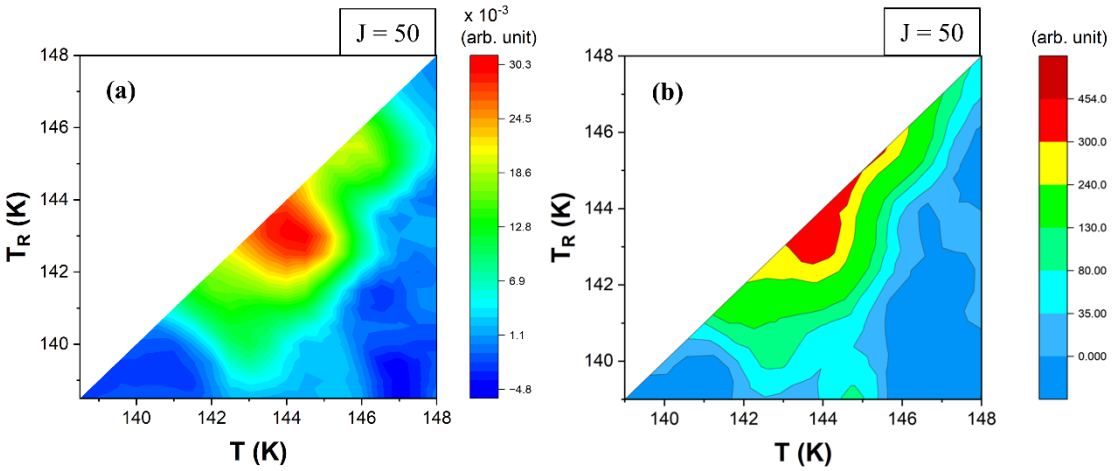


**Fig. 9:** Simulated calorimetric-type FORC diagrams in the heating mode for $\Delta S = 7$, $E_A = 400$ K, $k_B = 1$, $G = 0$, $\mu_\Delta = 1000$, with $\sigma_\Delta = 200$ and $J = 50$ a) using the standard FORC method, and b) by calculation from thermogram data.

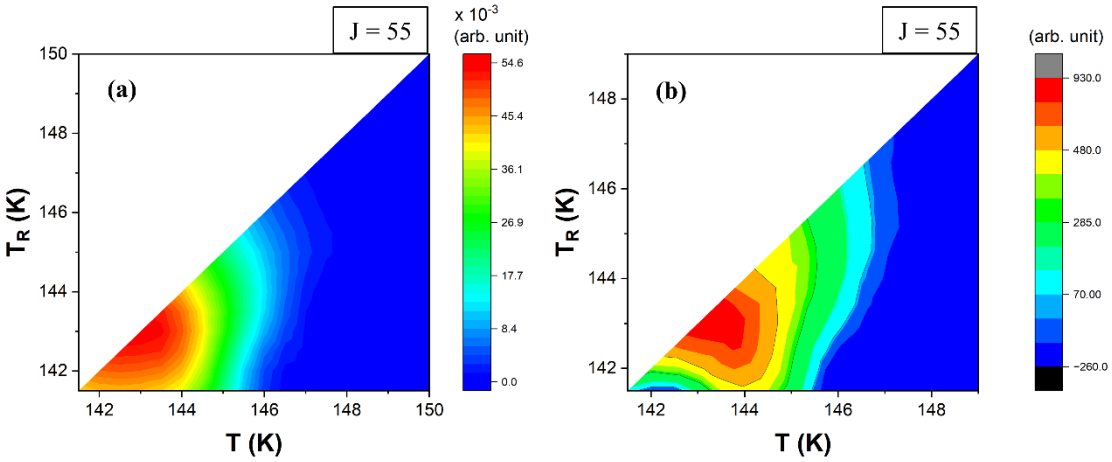


**Fig. 10:** Simulated calorimetric-type FORC diagrams in the heating mode for $\Delta S = 7$, $E_A = 400$ K, $k_B = 1$, $G = 0$, $\mu_\Delta = 1000$, with $\sigma_\Delta = 200$ and $J = 55$ a) using the standard FORC method and b) by calculation from thermogram data.

## CONCLUSIONS

In this paper, we have explored two complementary measuring techniques for characterizing the spin crossover compound $[Fe(btr)_2(NCS)_2]\cdot H_2O$ using the FORC method. For magnetometry, the FORC calculation requires a surface polynomial fitting, whereas in calorimetry, a single derivative is sufficient to determine the FORC distribution. Both methods lead to the same results. More broadly, the calorimetric approach simplifies diagram calculation when the reversal temperature step between successive cycles significantly differs from the measurement step within a single cycle. The Ising-like model successfully reproduces both experiments, and an original method to calculate the thermograms is introduced. This study has broader implications for composite materials research, where calorimetry can effectively distinguish between different phases. Calorimetric FORCs may also be a valuable experimental tool in the calorimetric studies of giant magnetocaloric effects in various materials. [23, 24]

## SUPPLEMENTARY INFORMATION

Sample characterization using calorimetry.

**ACKNOWLEDGEMENTS**

This work was financially supported by CNCS-UEFISCDI Romania (grant number PN-III-P4-ID-PCE-2020-1946).

## AUTHOR DECLARATIONS

### Conflict of Interest

The authors have no conflicts to disclose.

### Author Contributions

**Diana Plesca**: Data curation; Formal analysis; Investigation; Software; Visualization. **Cristian Enachescu**: Conceptualization; Methodology; Software; Writing – original draft. **Radu Tanasa**: Conceptualization; Formal analysis; Methodology; Writing – original draft; Writing – review & editing. **Alexandru Stancu**: Formal analysis; Writing – review & editing. **Denis Morineau**: Conceptualization; Data curation; Investigation; Writing – review & editing. **Marie-Laure Boillot**: Resources; Writing – review & editing.

## DATA AVAILABILITY

The data that support the findings of this study are available from the corresponding author upon reasonable request.

**REFERENCES**


1. C. R. Pike, A. P. Roberts and K. L. Verosub, Geophys. J. Int. **145**, 721 (2001).
2. A. Stancu, C. R. Pike, L. Stoleriu, P. Postolache and D. Cimpoesu, J. Appl. Phys. **93** (10), 6620-6622 (2003).
3. H. G. Katzgraber, F. Pazmandi, C. R. Pike, K. Liu, R. T. Scalettar, K. L. Verosub and G. T. Zimanyi, Phys. Rev. Lett. **89** (25), 257202 (2002).
4. A. Atitoaie, R. Tanasa, A. Stancu and C. Enachescu, J. Magn. Magn. Mater. **368**, 12-18 (2014).
5. R. M. Stan, R. Gaina, C. Enachescu, R. Tanasa, A. Stancu and R. Bronisz, J. Appl. Phys. **117** (17), 17B323 (2015).
6. L. Stoleriu, A. Stancu, P. Chakraborty, A. Hauser and C. Enachescu, J. Appl. Phys. **117** (17), 17B307 (2015).
7. I. Rusu, I. C. Manolache-Rusu, A. Diaconu, O. Palamarciuc, I. y. A. Gural'skiy, G. Molnar and A. Rotaru, J. Appl. Phys. **129** (6), 064501 (2021).
8. R. Tanasa, A. Stancu, E. Codjovi, J. Linares, F. Varret and J. F. Letard, J. Appl. Phys. **103**, 07B905 (2008).
9. K. Boukheddaden, S. Miyashita and S. Triki, J. Appl. Phys. **132** (22), 220402 (2022).
10. P. O. Ribeiro, B. P. Alho, E. P. Nobrega, V. S. R. de Sousa, A. M. G. Carvalho and P. J. von Ranke, J. Appl. Phys. **133** (12), 125104 (2023).
11. R. Tanasa, C. Enachescu, J. Laisney, D. Morineau, A. Stancu and M. L. Boillot, J. Phys. Chem. C **123** (15), 10120-10129 (2019).
12. R. Tanasa, C. Enachescu, A. Stancu, J. Linares, E. Codjovi, F. Varret and J. G. Haasnoot, Phys. Rev. B **71**, 014431 (2005).
13. R. Tanasa, C. Enachescu, A. Stancu, F. Varret, J. Linares and E. Codjovi, Polyhedron **26**, 1820-1824 (2007).
14. A. Andriesei, D. Plesca, R. Capu, R. M. Stan, R. Tanasa and C. Enachescu, Rom. Rep. Phys. **75** (3), 502 (2023).
15. D. Cimpoesu, I. Dumitru and A. Stancu, J. Appl. Phys. **125** (2), 023906 (2019).
16. I. Abou Hamad, D. T. Robb and P. A. Rikvold, J. Electroanal. Chem. **607** (1-2), 61-68 (2007).

17. W. Vreugdenhil, J. H. Van Diemen, R. A. G. De Graaff, J. G. Haasnoot, J. Reedijk, A. M. Van Der Kraan, O. Kahn and J. Zarembowitch, Polyhedron **9** (24), 2971-2979 (1990).

18. C. R. Pike, A. P. Roberts and K. L. Verosub, J. Appl. Phys. **85**, 6660 (1999).

19. A. Rotaru, M. M. Dirtu, C. Enachescu, R. Tanasa, J. Linares, A. Stancu and Y. Garcia, Polyhedron **28**, 2351-2356 (2009).

20. C. Enachescu, R. Tanasa, A. Stancu, E. Codjovi, J. Linares and F. Varret, Physica B **343**, 15-19 (2004).

21. I. Krivokapic, C. Enachescu, R. Bronisz and A. Hauser, Chem. Phys. Lett. **455**, 192 (2008).

22. D. Plesca, A. Railean, R. Tanasa, A. Stancu, J. Laisney, M. L. Boillot and C. Enachescu, Magnetochemistry **7** (5), 59 (2021).

23. E. Palacios, R. Burriel and C. L. Zhang, Phys. Rev. B **103** (10), 104402 (2021).

24. J. Y. Law, L. M. Moreno-Ramírez, Á. Díaz-García and V. Franco, J. Appl. Phys. **133** (4), 040903 (2023).